Atmos. Chem. Phys. Discuss., 10, 3229–3263, 2010
www.atmos-chem-phys-discuss.net/10/3229/2010/

Atmospheric Chemistry and Physics Discussions

This discussion paper is/has been under review for the journal Atmospheric Chemistry and Physics (ACP). Please refer to the corresponding final paper in ACP if available.

Ozone predictabilities due to meteorological uncertainties in Mexico City basin using ensemble forecasts

N. Bei[1], **W. Lei**[1], **M. Zavala**[1], **and L. T. Molina**[1,2]

[1]Molina Center for Energy and the Environment, La Jolla, CA, USA
[2]Department of Earth, Atmospheric and Planetary Sciences, Massachusetts Institute of Technology, Cambridge, MA, USA

Received: 8 January 2010 – Accepted: 11 January 2010 – Published: 5 February 2010

Correspondence to: N. Bei (bnf@mce2.org)

Published by Copernicus Publications on behalf of the European Geosciences Union.

Abstract

The purpose of the present study is to investigate the sensitivity of ozone concentration ($[O_3]$) predictions in Mexico City to meteorological initial uncertainties and planetary boundary layer (PBL) parameterization schemes using state-of-the-art meteorological and photochemical prediction models through ensemble forecasts. The simulated periods (3, 9, 15, and 29 March 2006), represent four typical meteorological episodes ("South-Venting", "O_3-North", "O_3-South" and "Convection-North", respectively) in the Mexico City basin during the MCMA-2006/MILAGRO campaign. Our results demonstrate that uncertainties in meteorological initial conditions have significant impacts on O_3 predictions, including the peak time $[O_3]$, as well as the horizontal and vertical $[O_3]$ distributions, and temporal variations. The ensemble spread of the simulated peak $[O_3]$ averaged over the city's ambient monitoring sites can reach up to 10 ppb. The magnitude of the ensemble spreads varies with different PBL schemes and meteorological episodes. The uncertainties in O_3 predictions caused by PBL schemes mainly come from their ability to represent the mixing layer height, but overall, these uncertainties are smaller than those from uncertainties in meteorological initial conditions.

1 Introduction

The predictability of the weather is inherently limited because of the chaotic nature of the atmosphere (Lorenz, 1969). The limited deterministic predictability in numerical weather prediction (NWP) has been extensively studied (see e.g., Leith and Kraichnan, 1972; Anthes et al. 1985; Errico and Baumhefner, 1987; Vukicevic and Errico, 1990; Zhang et al., 2002, 2003; Tribbia and Baumhefner, 2004; Zhang et al., 2006; Bei and Zhang, 2007). It has been found that the error grows with the background dynamics and this is strongly nonlinear. Smaller amplitude initial errors, which are far smaller than those of current observational networks, may grow rapidly and quickly saturate at smaller scales. These errors successively grow upscale, leading to significant forecast

ACPD

10, 3229–3263, 2010

uncertainties at increasingly larger scales. Besides, moist convection is found to be the key to the rapid error growth that leads to limited predictability at the mesoscales. Ensemble techniques are commonly used to improve the forecast ability of meteorological models (e.g., Kalnay, 2003) and have been successfully applied to dispersion forecasts of radionuclides and inert tracers (Galmarini et al., 2004, and references therein).

An ensemble forecast system is composed of multiple individual numerical forecasts (members) generated from a set of different initial conditions and/or different numerical configurations (Leith, 1974). In addition, probabilistic forecasts, which have been presented elsewhere (e.g., Buizza et al., 1993; Toth and Kalnay, 1993; Mullen and Buizza, 2002), can also be obtained from the relative frequencies of events represented in the ensemble.

Ensemble prediction systems have been widely used operationally in meteorological centers around the world, such as the National Centers for Environmental Prediction (NCEP) (Toth and Kalnay, 1993), the European Center for Medium-Range Weather Forecasts (ECMWF) (Buizza, 1997), and the Meteorological Service of Canada (MSC) (Houtekamer and Lefaivre, 1997). It has been found that the ensemble mean is more accurate than an individual model realization, when verified for numerous cases. NWP ensembles could be implemented by using different model initial conditions (Toth and Kalnay, 1993, 1997; Molteni et al., 1996), different parameterizations within a single model (Stensrud et al., 1998), different numerical schemes (Thomas et al., 2002), and different models (Hou et al., 2001; Wandishin et al., 2001). This allows the ensemble to consider different sources of uncertainty.

The ensemble technique can yield similar benefits to real-time air quality prediction, because there are similar model complexities and constraints. For example, a probabilistic approach to air quality forecasting has been recommended by the US Weather Research Program and its Prospectus Development Team on Air Quality Forecasting (Dabberdt et al., 2003) because of the chaotic nature of the atmosphere and chemistry nonlinearity. Delle Monache and Stull (2003) have discussed the benefits of the ensemble approach through the use of different Chemical Transport Models (CTMs) and the

ACPD
10, 3229–3263, 2010

associated photochemical reactions. Galmarini et al. (2004b) have tested a multimodel ensemble dispersion system by considering several operational long-range transport and dispersion models. They found that the median member of the forecast ensemble exhibited the best forecast skill. McKeen et al. (2005) have presented results for a multimodel (i.e., seven CTMs) Ozone Ensemble Forecast System (OEFS), statistically evaluated for 53 days against 340 monitoring stations over Eastern US and Southern Canada. Their results showed that the ensemble mean is the preferred forecast when compared to any individual model. Mallet and Sportisse (2006) have conducted the ensemble photochemical simulations by using different physical parameterizations. Delle Monache et al. (2006a) have tested a new OEFS to improve the accuracy of real-time photochemical air quality modeling using different meteorological and photochemical models together with different emission scenarios. In all cases, the ensemble means perform better than most models individually.

Recent studies have also demonstrated that the air quality forecasts can be further improved through weighted ensemble means (e.g., Delle Monache et al., 2006b; Pagowski et al., 2005). Using both meteorological and photochemical ensemble forecasts, it has been shown that there are large uncertainties in the ozone prediction in Houston and surrounding areas due to initial meteorological uncertainties (Zhang et al., 2007). This further demonstrates the importance of accurate representation of meteorological conditions and the need for probabilistic evaluation and forecasting for air pollution in urban areas. The ozone prediction sensitivities due to PBL schemes through deterministic forecast have been conducted by Mao et al. (2006). Their results show that the option of PBL schemes in MM5 does not appreciably affect the CMAQ performance when the evaluations are averaged throughout the entire modeling domain. However, on an urban scale the differences in O_3 prediction across different PBL schemes are considerable.

The Mexico City Metropolitan Area (MCMA) is situated inside a basin at an elevation of 2240 m above sea level (a.s.l.) at 19.4° N latitude and is surrounded on three sides by mountains averaging over 3000 m a.s.l. (see Fig. 1b). The main opening of

ACPD
10, 3229–3263, 2010

the basin is towards the Mexico Plateau to the north. To the southeast there is a gap in the mountains, referred to as the Chalco passage, which leads to significant gap winds. The combination of weak winds and numerous emission sources results in high levels of air pollution (Molina and Molina, 2002). Because of its complex topography, the meteorology of the MCMA depends on the interplay of the basin with the Mexica Plateau and the lower coastal areas (along the eastern Pacific Ocean and the Gulf of Mexico). Both regional and synoptic-scale meteorological conditions are important for understanding flows and dispersions within the Mexico City basin (Bossert, 1997). The complex wind circulation in the Mexico City basin and its role in the formation of surface air pollution distributions in the basin have been analyzed extensively in previous studies (e.g., Wellens et al., 1994; Williams et al., 1995; Streit and Guzman, 1996; Jauregui, 1997; Fast and Zhong, 1998; Doran and Zhong, 2000; Jazcilevich et al., 2003; de Foy et al. 2005, 2006a, b, 2008). Tie et al. (2007) used a newly developed regional chemical/dynamical model (WRF-Chem) to study the formation of chemical oxidants, particularly ozone in Mexico City. As a major field study investigating the atmospheric chemistry of the MCMA, the MCMA-2003 campaign revealed important new insights into the meteorology, primary pollutant emissions, ambient secondary pollutant precursor concentrations, photochemical oxidant production, and secondary aerosol particle formation in North America's most populated megacity (Molina et al., 2007).

To better understand the evolution of trace gases and particulates originating from anthropogenic emissions in the MCMA and their impact on regional air quality and climate, a field campaign called the Megacities Initiative: Local And Global Research Observations (MILAGRO) collected a wide range of meteorological, gaseous and particulate measurements during March 2006 (Molina et al., 2008). Fast et al. (2007) described the large-scale meteorological conditions that affected atmospheric chemistry over Mexico during March 2006 and defined three regimes that characterized the overall meteorological conditions: the first regime prior to 14 March, the second regime between 14 and 23 March, and the third regime after 23 March. de Foy et al. (2008) used cluster analysis to identify the dominant wind patterns in the Mexico City basin

both during the campaign and within the past 10 years of operational data from the warm dry season. Six episodes were identified for the basin-scale circulation, which includes "O_3-South", "O_3-North", "Cold Surge", "South-Venting", "Convection-South", and "Convection-North". Bei et al. (2008) investigated the effects of using a 3DVAR data assimilation system in meteorological modeling to improve [O_3] simulations in the Mexico City basin during the MCMA-2003 campaign, and demonstrated the importance of applying data assimilation in meteorological simulations of air quality in the Mexico City basin. Still, there are discrepancies between ozone predictions and observations due to meteorological field simulations for some of the days (Lei et al., 2007, 2008).

The purpose of this study is to investigate the uncertainties of ozone predictions in the Mexico City basin due to meteorological uncertainties, which arise from initial conditions and PBL parameterization schemes. The impacts of meteorological uncertainties on ozone predictability are investigated through ensemble forecasts using state-of-the-art meteorological and photochemical prediction models for four selected days (3, 9, 15, and 29 March 2006) that represent four typical meteorological episodes ("South-Venting", "O_3-North", "O_3-South", and "Convection-North") in O_3 predictions in the Mexico City basin during MILAGRO/MCMA-2006 (de Foy et al., 2008). The models and experimental designs are presented in Sect. 2. The synoptic situations of the selected days are overviewed in Sect. 3. The control ensemble forecasts are introduced in Sect. 4. The ensemble forecasts with different PBL schemes and ensemble simulations on other three days are presented in Sects. 5 and 6, respectively; the conclusions are summarized in Sect. 7.

2 Forecast models, ensemble generation, and experimental design

The Advanced Research WRF (ARW) (WRF v2.2.1; Skamarock et al., 2005) is used in meteorological deterministic and ensemble forecasts. The model simulations adopt three one-way nested grids with horizontal resolutions of 36, 12, and 3 km and 35 sigma levels in the vertical direction (Fig. 1a). The grid cells used for the three domains

ACPD
10, 3229–3263, 2010

are 145×95, 259×160, and 193×193, respectively. The WRF model is initialized at 00:00 UTC and integrated for 30 h. The physical process parameterization schemes used in the reference deterministic forecasts include the modified Kain-Fritsch cumulus scheme (KF-Eta) (Kain and Fritsch, 1993), the WRF Single Moment (WSM) three-class microphysics (Hong et al., 2004), and Mellor-Yamada-Janjic Eta Model (ETA) (Janjic, 2002) for PBL processes. The NCEP global final (FNL) analysis are used to create the initial and boundary conditions.

The initial ensemble is generated with the WRF-3DVAR (Barker et al. 2004) using BES option cv5. A set of random control vectors with a normal distribution was generated. The control increment vector is then transformed back to model space via an empirical orthogonal functions (EOF) transform, a recursive filter, and physical transformation via balance equation. The perturbed variables include the horizontal wind components, potential temperature, perturbation pressure, and mixing ratio for water vapor whose error statistics are defined by the domain-specific climatological background error covariance, which are derived from the one-month simulations in the same domain using the NMC method (Parrish and Derber, 1992). Other prognostic variables such as vertical velocity (w) and mixing ratios for cloud water (q_c), rain water (q_r), snow (q_s) and graupel (q_g) are not perturbed.

Figure 2 shows the vertical distribution of the initial ensemble spread, which is 0.4–1.3 m/s for horizontal winds (u, v), 0.3–1.0 K for temperature (T), 0–0.4 hPa for pressure (p), and 0–1.2 g/kg for the water vapor mixing ratio (q). The 3DVAR perturbations are added to the GFS FNL analysis to form an initial ensemble, which is then integrated for 30 h to produce the ensemble forecasts. The perturbations created through this method are basically balanced and large scale; and their magnitude are also small compare to the typical sounding observational and analysis errors (Nielsen-Gammon et al., 2007). Similar methods to generate the initial ensemble are also employed by Meng and Zhang (2008) and Barker (2005). The boundary conditions (created by the GFS analysis at different times) are perturbed in the same manner as the initial ensemble.

ACPD
10, 3229–3263, 2010

The 3-km meteorological ensemble simulations are then used to drive a 20-member photochemical ensemble forecast using the Eulerian photochemical grid model CAMx v4.40 (Environ, 2006). The CAMx model domain (70×70 grids, Fig. 1b) is much smaller than the WRF domain 3 because of available computing resources and emissions data. The model set-up and the input data used for CAMx in this study are the same as those described in Song et al. (2009) except the meteorological fields. The emission input is constructed based on the official MCMA emissions inventory for the year 2006 (SMA-DF, 2008) and is adjusted based on comprehensive field measurements of O_3 precursors, as described in Song et al. (2009). For all the experiments, the initial and boundary conditions for chemical fields are the same, since we only focus on the effects due to changes in the meteorological fields.

Both meteorological and photochemical ensemble forecasts are conducted on four selected days (3, 9, 15, and 29 March 2006). We choose 3 March as a control ensemble run (CTRL), and most analyses will only be conducted on this day since we believe that the selected day will not affect our results. The physical process parameterization schemes used in the CTRL run are the same as those used in the reference deterministic forecast.

Uncertainties in air quality modeling arise when different physical parameterization schemes are used in meteorological models (see, e.g., Alapaty et al., 1994; Pielke and Uliasz, 1998). One of the most important meteorological parameters that affect the uncertainties in models predictions is the planetary boundary layer. We study the impact of PBL parameterization schemes on the ozone simulation of 3 March 2006 by conducting ensemble forecasts using other two different PBL schemes (PBL2 and PBL3 described below), which include the Yonsei University (YSU) scheme (Noh et al., 2003) and the Medium-Range Forecast (MRF) model (Hong and Pan, 1996).

ACPD
10, 3229–3263, 2010

3 Overview of the synoptic conditions

The four days selected in this paper represent four different meteorological episodes types in Mexico City. 3 March is a "South-Venting" day, which represents northeasterly winds aloft and strong southward transport at the surface. There is an anti-cyclone on 700 hPa over the border of Mexico and US (Fig. 3a), which leads to northeasterly wind over the Mexico City basin. The prevailing southerly winds on surface are affected by the high pressure system on the north (Fig. 4a). 9 March represents an "O_3-North" day, which has stronger southwesterly winds over the basin rim and a north-south convergence zone. On that day, there is an anti-cyclone located at southwest of Mexico on 700 hPa (Fig. 3b), leading to a divergence zone over Mexico City. During the daytime, there is a weak surface high over Mexico City, which is finally replaced by the local wind circulation (Fig. 4b). 15 March is an "O_3-South" day when an anticyclone on 700 hPa is located in the Gulf of Mexico (Fig. 3c), resulting in the southeasterly wind aloft. Northerly surface winds in the morning (not shown) meet the southeast gap flow in the afternoon (Fig. 4c), which leads to an east-west convergence zone moving northwards in the evening. 29 March is classified as "Convection-North", which represents weak southerly wind aloft and rain in the northern part of the basin. There is an anti-cyclone on 700 hPa over Mexico (Fig. 3d), which leads to subsidence over Mexico City basin. The wind circulation on the surface is mostly affected by the local topography (Fig. 4d). The convergence develops in daytime while the divergence occurs in nighttime and early morning due to the surrounding mountain area.

4 Control ensemble simulation

4.1 Overview of the control ensemble performance

Figure 5 shows the time evolution of the ensemble mean and spread of the surface $[O_3]$ for the average at the Ambient Air Monitoring Network sites (squares shown in Fig. 1b, referred as RAMA sites in the following text) in the Mexico City basin and the

ACPD
10, 3229–3263, 2010

selected five single stations (XAL, CES, MER, PED, and TLA, denoted in Fig. 1b). Two highlighted members (bold green lines in Fig. 5a) are EN-11 and EN-14, which represent a low [O_3] case and a high [O_3] case, which will be discussed in the following section. For both the average and the single stations, the ensemble mean captures reasonably well the sharp buildup of [O_3] in the morning. However, the ensemble mean tends to overestimate the [O_3] during the afternoon on this day, especially during the peak ozone period. The ensemble spread of simulated surface [O_3] averaged over the RAMA sites can reach up to 10 ppb (Fig. 5a) during the peak time period. In general, the ensemble spread is much bigger at the selected five single stations (Fig. 5b–f), with the maximum of more than 15 ppb. The observations are principally within the spread of the ensemble simulations, while the ensemble mean is slightly higher than the observations but generally better than the reference deterministic forecast. It indicates that shortage still exist in the ensemble simulation.

Figure 6 shows the evolution of the ensemble mean of the surface ozone distributions along with the ensemble mean wind vectors in Mexico City basin and the surrounding area simulated by the CNTL ensemble. At the initial time (00:00 CDT), the lower ensemble mean ozone area is located within the urban area of the Mexico City basin due to the titration from NO emissions and the lack of photochemical activities and continues towards the early morning (06:00 CDT). From 06:00 to 12:00 CDT, the ozone level starts to elevate inside the basin with the increased southerly winds, mainly due to increasing photochemical activities. From 12:00 to 15:00 CDT, in association with the increase of northerly wind, a convergence zone is formed in the southwest of Mexico City basin, leading to the occurrence of maximum [O_3] inside the basin around 15:00 CDT, which is consistent with the observations from the RAMA sites (squares). From 15:00 to 18:00 CDT, the high ensemble mean ozone area moves southward along with the increased northerly winds. Toward the end of the day (21:00 CDT), the ensemble mean of ozone decreases again inside the basin.

Figure 7 shows the surface winds measured at the RAMA sites along with the simulated ensemble mean surface winds in the basin around peak time. In general, the

ensemble mean of surface winds agree better with the measurements inside the basin than those in the surroundings. However, the discrepancies between the ensemble mean and observations are still obvious, which could be caused by the systematic errors in initial conditions and uncertainties in meteorological models. Another important reason could be the 3-km horizontal resolution adopted in our simulations. Basically, the effective resolution in numerical simulations is about 7 times of the horizontal resolution used in the model (Skamarock, 2004), which is 21 km in our case. It should be noted that the distances between most of the RAMA sites are less than 21 km, therefore higher-resolution simulations might be necessary to more accurately simulate the basin scale phenomenon.

4.2 Uncertainties during the peak ozone period

Although the initial meteorological uncertainties used in our study (see Fig. 2) are smaller than typical observational and analysis errors, our ensemble forecasts demonstrate large uncertainties in ozone prediction, especially during peak ozone period (12:00–18:00 CDT), are possible during the peak time period (see Fig. 5a).

To illustrate the discrepancy between different ensemble members, we have selected two ensemble members: EN-11 and EN-14, which represent the lowest and highest [O_3] averaged over 19 RAMA sites, respectively (bold green lines shown in Fig. 5a). Figure 8 presents the horizontal distribution of surface [O_3] along with surface winds from EN-11 and EN-14. There are obvious differences in the surface winds between these two extreme members, which are also closely related to the dramatic difference in ozone distributions in Mexico City basin. The surface winds have stronger (weaker) northwesterly component in EN-11 (EN-14) before peak ozone time (Fig. 8a and b) in the northwest of the basin, which results in less (more) ozone precursors inside the Mexico City basin in EN-11 (EN-14). At the peak time (Fig. 8c and d), the northwesterly surface winds are still stronger (weaker) in EN-11 (EN-14) in the northwest of the basin and the southerly gap winds are weaker (stronger) in EN-11 (EN-14), which leads to less (more) ozone precursors and lower (higher) ozone inside the basin in EN-11

(EN-14). After the peak time (Fig. 8e and f), the high ozone area in both case has been moved outside of the basin.

The vertical distributions of [O_3], potential temperature, wind vectors, and PBL height further demonstrate the large differences between EN-11 and EN-14 (Fig. 9). Before peak ozone time (upper panels), both southeasterly low-level winds and northwesterly upper-level winds are stronger (weaker) in EN-11 (EN-14) over the basin, causing less (more) ozone precursors inside the Mexico City basin in EN-11 (EN-14). At the peak time (middle panels), both low-level winds and upper-level winds remain stronger in EN-11 than in EN-14 and thence more ozone precursors are transported outside of the basin in EN-11 than in EN-14. More ozone precursors and higher temperature in EN-14 are favorable for the O_3 formation in the basin. After the peak time (bottom panels), the plumes in both members start to decay due to the intensified upslope winds.

4.3 Connections between meteorological uncertainties and ozone prediction uncertainties

Meteorological conditions, such as wind fields, temperature, water vapor mixing ratio, and boundary layer height are known to have direct impacts on the air quality simulation (Seaman, 2000). The ensemble simulations are a good technique to examine the relationship between the uncertainties in meteorological fields and the uncertainties in ozone simulations. To evaluate the model results we interpolate the model output variables (PBL height, wind speed, and surface temperature) to the location of the 19 RAMA sites (shown in Fig. 1b) and then calculate the average. Figure 10 shows the time evolution of PBL height, wind speed, and surface temperature from the initial time of the meteorological model (6 h earlier than the initial time of the photochemical model). The ensemble spread of these variables among different members is initially small but gradually grows along the integration time. However, during the morning hours (06:00–12:00 CDT), the ensemble spread of the above-mentioned meteorological variables is relatively small compare with other periods during the simulation time, leading to the smaller ensemble spread of [O_3] for this period. During peak ozone

period (12:00–18:00 CDT), the maximum ensemble spreads of the wind speed, PBL height, and surface temperature are around 1.25 m s^{-1}, 0.5 km, and 1.5 K, respectively, and are much larger than those during other periods, demonstrating that the large ozone prediction uncertainties are attributed to the large meteorological uncertainties. The ensemble spreads of PBL heights and wind speeds start to increase from 12:00 CDT, which correspond well to the enhancement of the ensemble spread of [O_3]. The PBL height and wind speed affect the surface [O_3] through vertical and horizontal transport of pollutants. The convergence caused by the wind circulation determines the location and affects the level of the high ozone area as mentioned in the previous section. All these factors are combined together to affect the ozone distributions. For example, we have highlighted (brown lines) the two extreme members (EN-11 and EN-14). For the low ozone case (EN-11), it has lower PBL height, higher wind speed, and lower surface temperature, which act together to lower [O_3] in EN-11. The high ozone case (EN-14) has higher PBL height, lower wind speed, and higher surface temperature.

5 Effects of PBL parameterization schemes

In order to investigate the impact of PBL parameterization schemes on the ozone simulation, we have conducted ensemble forecasts using two other PBL schemes, the YSU scheme (Noh et al., 2003) and the MRF scheme (Hong and Pan, 1996) in addition to the ETA scheme used in the control case.

Figure 11 shows the time evolution of simulated surface [O_3] averaged over the RAMA sites using the YSU (PBL2) and MRF schemes (PBL3). The differences in ozone simulations between different PBL schemes mainly remain at night and early morning hours (00:00–06:00 CDT) and peak ozone hours (12:00–18:00 CDT). The ozone simulations during the morning hours are poorly simulated using YSU scheme and MRF scheme, while the ozone simulation by ETA scheme (control run) during this period is better (Fig. 5a). The MRF scheme has the highest peak [O_3] while the ETA

ACPD
10, 3229–3263, 2010

scheme has the lowest peak [O_3]. The ensemble spread of simulated surface [O_3] averaged over the RAMA sites also varies with different PBL schemes. The ensemble spread of peak time [O_3] with the YSU scheme is slightly smaller than that with MRF scheme but larger than that with ETA scheme. The ensemble mean between different PBL schemes shows a difference of 2–5 ppb during peak time, which is clearly less than those from initial condition uncertainties. The time evolution of PBL height, wind speed, and surface temperature using other two PBL schemes is shown in Fig. 12. It can be seen that the MRF scheme has larger spreads of the PBL height, wind speed, and surface temperature (Fig. 12b, d, and f) than the YSU scheme, which causes correspondingly a larger spread of ozone simulations (Fig. 11b) in the afternoon.

6 The ensemble simulations on other episodes

In order to explore the impacts of meteorological uncertainties on O_3 predictability under different meteorological conditions, we have further conducted ensemble forecasts on 9, 15, and 29 March that represent three other typical ozone pollution episodes ("O_3-North", "O_3-South" and "Convection-North") in Mexico City basin (de Foy et al., 2008), using both meteorological and photochemical models.

Figure 13 shows the time evolution of simulated surface [O_3] averaged over the RAMA sites versus the observations on these three days. The time evolution of ensemble mean basically agrees well with the observations. The ensemble mean is mostly better than the reference deterministic forecast (such as 9 and 29 March), but the ensemble spread varies in different episodes. The maximum ensemble spreads during the peak ozone hours on 9, 15, and 29 March are 8 ppb, 5 ppb, and 7 ppb, respectively, slightly smaller than that of 3 March, but still significant in comparison with the ensemble mean.

The ozone predictability for different episodes seems different, e.g., 15 March has the smallest spread during the peak ozone period. As mentioned in Sect. 3, 15 March is an "O_3-SOUTH" day, which has weak synoptic forcing and a much clearer signature

of terrain-induced flow (such as gap flow). The initial perturbations adopted in our ensemble system mostly focus on the large scale, which did not reflect the small scale initial error very well. The ensemble mean [O_3] is almost the same as the reference deterministic forecast during the peak ozone period. The discrepancy between ensemble mean and the observations on this day is also larger than the other 3 days.

While the ensemble mean can provide better magnitude of simulated [O_3], the timing of the peak ozone is only slightly improved on these days. The possible reason could be the model error or emission uncertainties as described in the previous section since meteorological initial condition uncertainty is only one of several known sources of significant photochemical model errors (Hanna et al., 2001).

7 Conclusions

We have investigated the ozone predictability due to meteorological uncertainties in the meteorological simulation by conducting meteorological and photochemical ensemble simulations in Mexico City basin on four selected days. We focus on the uncertainties in the meteorological simulations caused by initial condition error and PBL schemes. The initial ensemble is generated with the WRF-3DVAR. The error statistics are defined by the domain-specific climatological background error covariance, which are derived from one-month simulations in the same domain using NMC method. The four days selected (3, 9, 15, and 29 March 2006) represent four different meteorological episodes in Mexico City basin. We choose 3 March 2006 as a control run to analyze the results.

Over the 24-h simulation, the ensemble means compare fairly well with the observations, including the maximum [O_3], the buildup of [O_3] in the early afternoon, and the transport of the plume. However, there are still discrepancies between the ensemble mean and the observations, which can be explained by the systematic errors in initial condition and uncertainties in both meteorological and photochemical models, as well as uncertainties in the emission inventory. Horizontal resolution used in the current study may also be a limiting factor for investigating the basin scale phenomenon. We plan to focus on these problems in our future work.

The increasing uncertainties in meteorological fields during the peak ozone period contribute to the unpredictablity in ozone simulations. However, the relationship between the uncertainties in meteorological fields and ozone prediction are flow-dependent and also complicated. Basically, the impact of wind speed and PBL height on [O_3] are more straightforward, such as through horizontal and vertical transport of pollutants, while the impact of temperature and water vapor are generally indirect. These factors combine to affect the ozone distributions.

The uncertainties in the ozone prediction, especially during the peak ozone period, in Mexico City basin due to meteorological factors are mainly from initial condition uncertainties. The magnitude of the ensemble spread also varies with different PBL schemes, which affect the PBL height, wind, and temperature; these in turn affect the O_3 simulations. The differences in ozone simulations using different PBL schemes mainly occur during nighttime and early morning hours and peak ozone hours. In addition, the ensemble spread of surface ozone varies with different meteorological episodes and is significant compared with the ensemble mean.

However, even with ample observations, analysis inaccuracies are also inevitable. Therefore, a single-minded pursuit of improved initial conditions is not advisable; instead, ensemble simulations should be used to span the range of possible outcomes consistent with the meteorological conditions on a given day. An ensemble forecasting system, incorporating as many sources of error (such as uncertainties in initial conditions and models) as possible, can provide guidance on both the most likely ozone evolution and also the range of possibilities.

Acknowledgement. We are indebted to the large number of people involved in the MILAGRO field campaign as well as those involved in long-term air quality monitoring and the emissions inventory in the Mexico City metropolitan area, which made this study possible. The authors gratefully acknowledge financial support from the US National Science Foundation (ATM-0810931). We would like to thank Yonghui Weng at Texas A&M University and Zhiyong Meng at Peking University for their help in the implementation of the ensemble simulations. Acknowledgment is also made to the National Center for Atmospheric Research, which is sponsored by the National Science Foundation, for the computing time used in this research.

References

Anthes, R. A., Kuo, Y. H., Baumhefner, D. P., Eriico, R. P., and Bettge, T. W.: Predictability of mesoscale of atmospheric motions, Adv. Geophys., 28B, 159–202, 1985.

Alapaty, K., Raman, S., and Madala, R. V.: Investigation of the role of the boundary layer processes in an active monsoon using a mesoscale model, Bound.-Lay. Meteorol., 67, 407–426, 1994.

Barker, D. M., Huang, W., Guo, Y.-R., Bourgeois, A. J., and Xiao, Q. N.: A three-dimensional variational data assimilation system for MM5: implementation and initial results, Mon. Weather Rev., 132, 897–914, 2004.

Barker, D. M.: Southern high-latitude ensemble data assimilation in the Antarctic mesoscale prediction system, Mon. Weather Rev., 133, 3431–3449, 2005.

Bei, N. and Zhang, F.: Impacts of initial condition errors on mesoscale predictability of heavy precipitation along the Mei-Yu front of China, Q. J. Roy. Meteor. Soc., 133, 83–99, 2007.

Bei, N., de Foy, B., Lei, W., Zavala, M., and Molina, L. T.: Using 3DVAR data assimilation system to improve ozone simulations in the Mexico City basin, Atmos. Chem. Phys., 8, 7353–7366, 2008, http://www.atmos-chem-phys.net/8/7353/2008/.

Bossert, J. E.: An investigation of flow regimes affecting the Mexico City region, J. Appl. Meteorol., 36, 119–140, 1997.

Buizza, R., Tribbia, J., Molteni, F., and Palmer, T.: Computation of optimal unstable structures for a numerical weather prediction model, Tellus, 45A, 388–407, 1993.

Buizza, R.: Potential forecast skill of ensemble prediction and spread and skill distributions of the ECMWF ensemble prediction system, Mon. Weather Rev., 125, 99–119, 1997.

Dabberdt, W. F., Carroll, M. A., Baumgardner, D., et al.: Meteorological research needs for improved air quality forecasting: Report of the 11th Prospectus Development Team of the US Weather Research Program, technical report, Natl. Cent. For Atmos. Res., Boulder, CO, 2003.

de Foy, B., Caetano, E., Magaña, V., Zitácuaro, A., Cárdenas, B., Retama, A., Ramos, R., Molina, L. T., and Molina, M. J.: Mexico City basin wind circulation during the MCMA-2003 field campaign, Atmos. Chem. Phys., 5, 2267–2288, 2005, http://www.atmos-chem-phys.net/5/2267/2005/.

de Foy, B., Clappier, A., Molina, L. T., and Molina, M. J.: Distinct wind convergence patterns in the Mexico City basin due to the interaction of the gap winds with the synoptic flow, Atmos.

Chem. Phys., 6, 1249–1265, 2006a, http://www.atmos-chem-phys.net/6/1249/2006/.
de Foy, B., Varela, J. R., Molina, L. T., and Molina, M. J.: Rapid ventilation of the Mexico City basin and regional fate of the urban plume, Atmos. Chem. Phys., 6, 2321–2335, 2006b, http://www.atmos-chem-phys.net/6/2321/2006/.
de Foy, B., Fast, J. D., Paech, S. J., Phillips, D., Walters, J. T., Coulter, R. L., Martin, T. J., Pekour, M. S., Shaw, W. J., Kastendeuch, P. P., Marley, N. A., Retama, A., and Molina, L. T.: Basin-scale wind transport during the MILAGRO field campaign and comparison to climatology using cluster analysis, Atmos. Chem. Phys., 8, 1209–1224, 2008, http://www.atmos-chem-phys.net/8/1209/2008/.
Delle Monache, L. and Stull, R.: An ensemble air quality forecast over western Europe during an ozone forecast, Atmos. Environ., 37, 3469–3474, 2003.
Delle Monache, L., Deng, X., Zhou, Y., and Stull, R.: Ozone ensemble forecasts: 1: A new ensemble design, J. Geophys. Res., 111, D05307, doi:10.1029/2005JD006310, 2006a.
Delle Monache, L., Nipen, T., Deng, X., Zhou, Y., and Stull, R.: Ozone ensemble forecasts: 2: a Kalman-filter predictor bias correction, J. Geophys. Res., 111, D05038, doi:10.1029/2005JD006311, 2006b.
Doran, J. C. and Zhong, S.: Thermally driven gap winds into the Mexico City basin, J. Appl. Meteorol., 39, 1330–1340, 2000.
ENVIRON International Corporation: Users Guide to the Comprehensive Air Quality. Model with Extensions (CAMx) version 4.40, available at: http://www.camx.com, 2006.
Errico, R. M. and Baumhefner, D. P.: Predictability experiments using a high-resolution limited-area model, Mon. Weather Rev., 115, 488–504, 1987.
Fast, J. D. and Zhong, S.: Meteorological factors associated with inhomogeneous s within the Mexico City basin, J. Geophys. Res., 103, 18927–18946, 1998.
Fast, J. D., de Foy, B., Acevedo Rosas, F., Caetano, E., Carmichael, G., Emmons, L., McKenna, D., Mena, M., Skamarock, W., Tie, X., Coulter, R. L., Barnard, J. C., Wiedinmyer, C., and Madronich, S.: A meteorological overview of the MILAGRO field campaigns, Atmos. Chem. Phys., 7, 2233–2257, 2007, http://www.atmos-chem-phys.net/7/2233/2007/.
Galmarini, S., Bianconi, R., Addis, R., et al.: Ensemble dispersion forecasting – Part I: Concept, approach and indicators, Atmos. Environ., 38, 4607–4617, 2004a.

Galmarini, S., Bianconi, R., Klug, W., et al.: Ensemble dispersion forecasting – Part II: Application and evaluations, Atmos. Environ., 38, 4619–4632, 2004b.
Hanna, S. R., Lu, Z. G., Frey, H. C., Wheeler, N., Vukovich, J., Arunachalam, S., Fernau, M., and Hansen, D. A.: Uncertainties in predicted ozone concentrations due to input uncertainties for the UAM-V photochemical grid model applied to the July 1995 OTAG domain, Atmos. Environ., 35, 891–903, 2001.
Hong, S. Y. and Pan, H.-L.: Nonlocal boundary layer vertical diffusion in a medium-range forecast model, Mon. Weather Rev., 124, 2322–2339, 1996.
Hong, S. Y., Dudhia, J., and Chen, S. H.: A revised approach to ice microphical processes for the bulk parameterization of clouds and precipitation, Mon. Weather Rev., 132, 103–120, 2004.
Hou, D., Kalnay, E., and Droegemeier, K. K.: Objective verification of the SAMEX'98 ensemble forecasts, Mon. Weather Rev., 129, 73–91, 2001.
Houtekamer, P. L. and Lefaivre, L.: Using ensemble forecasts for model validation, Mon. Weather Rev. 125, 2416–2426, 1997.
Janjić, Z. I.: Nonsingular implementation of the Mellor–Yamada level 2.5 scheme in the NCEP Meso Model. NCEP Office Note, 437, 61 pp., 2002.
Jauregui, E.: Heat island development in Mexico City, Atmos. Environ., 31, 3821–3831, 1997.
Jazcilevich, A. D., Garcia, A. R., and Ruiz-Suarez, L. G.: A study of air flow patterns affecting pollutant concentrations in the Central Region of Mexico, Atmos. Environ., 37, 183–193, 2003.
Kain, J. S. and Fritsch, J. M.: Convective parameterization for mesoscale models: The Kain–Fritsch scheme. The representation of cumulus convection in numerical models, Meteor. Mon., 46, 165–170, 1993.
Kalnay, E.: Atmospheric Modeling, Data Assimilation and Predictability, Cambridge Univ. Press, New York, 341 pp., 2003.
Lei, W., de Foy, B., Zavala, M., Volkamer, R., and Molina, L. T.: Characterizing ozone production in the Mexico City Metropolitan Area: a case study using a chemical transport model, Atmos. Chem. Phys., 7, 1347–1366, 2007, http://www.atmos-chem-phys.net/7/1347/2007/.
Lei, W., Zavala, M., de Foy, B., Volkamer, R., and Molina, L. T.: Characterizing ozone production and response under different meteorological conditions in Mexico City, Atmos. Chem. Phys., 8, 7571–7581, 2008, http://www.atmos-chem-phys.net/8/7571/2008/.

ACPD
10, 3229–3263, 2010

Leith, C. E. and Kraichnan, R. H.: Predictability of turbulent flows, J. Atmos. Sci., 29, 1041–1058, 1972.
Leith, C. E.: Theoretical skill of Monte Carlo forecasts, Mon. Weather Rev., 102, 409–418, 1974.
Lorenz, E. N.: The predictability of a flow which possesses many scales of motion, Tellus, 21, 289–307, 1969.
Mallet, V. and Sportisse, B.: Uncertainty in a chemistry-transport model due to physical parameterizations and numerical approximations: an ensemble approach applied to ozone modeling, J. Geophys. Res., 111, D01302, doi:10.1029/2005JD006149, 2006.
Mao, Q., Gautney, L. L., Cook, T. M., Jacobs, M. E., Smith, S. N., and Kelsoe, J. J.: Numerical experiments on MM5-CMAQ sensitivity to various PBL schemes, Atmos. Environ., 40, 3092–3110, 2006.
McKeen, S. A., Wilczak, J., Grell, G., et al.: Assessment of an ensemble of seven real-time ozone forecast over eastern North America during the summer of 2004, J. Geophys. Res., 110, D21307, doi:10.1029/2005JD005858, 2005.
Meng, Z. and Zhang, F.: Tests of an ensemble Kalman filter for mesoscale and regional-scale data assimilation. Part III: Comparison with 3DVAR in a real-data case study, Mon. Weather Rev., 136, 522–540, 2008.
Molina, L. T. and Molina, M. J. (Eds.): Air Quality in the Mexico Megacity: An Integrated Assessment, Kluwer Academic Publishers, 137–212, 2002.
Molina, L. T., Kolb, C. E., de Foy, B., Lamb, B. K., Brune, W. H., Jimenez, J. L., Ramos-Villegas, R., Sarmiento, J., Paramo-Figueroa, V. H., Cardenas, B., Gutierrez-Avedoy, V., and Molina, M. J.: Air quality in North America's most populous city – overview of the MCMA-2003 campaign, Atmos. Chem. Phys., 7, 2447–2473, 2007, http://www.atmos-chem-phys.net/7/2447/2007/.
Molina, L. T., Madronich, S., Gaffney, J. S., and Singh, H. B.: Overview of MILAGRO/INTEX-B campaign, in IGACtivities Newsletter of the International Global Atmospheric Chemistry Project, 38, 2–15 April 2008.
Molteni, F., Buizza, R., Palmer, T. N., and Petroliagis, T.: The new ECMWF ensemble prediction system: Methodology and validation, Q. J. Roy. Meteor. Soc., 122, 73–119, 1996.
Mullen, S. L. and Buizza, R., The impact of horizontal resolution and ensemble size on probabilistic forecasts of precipitation by the ECMWF Ensemble Prediction System, Weather Forecast., 17, 173–191, 2002.

ACPD
10, 3229–3263, 2010

Nielsen-Gammon, J. W., McNider, R. T., Angevine, W. M., White, A. B., and Knupp, K.: Mesoscale model performance with assimilation of wind profiler data: Sensitivity to assimilation parameters and network configuration, J. Geophys. Res., 112, D09119, doi:10.1029/2006JD007633, 2007.

Noh, Y., Cheon, W.-G., Hong, S.-Y., and Raasch, S.: Improvement of the K-profile model for the planetary boundary layer based on large eddy simulation data, Bound.-Lay. Meteorol., 107, 401–427, 2003.

Pagowski, M., Grell, G. A., Mckeen, S. A., et al.: A simple method to improve ensemble-based ozone forecasts, Geophys. Res. Lett., 32, L07814, doi:10.1029/2004GL022305, 2005.

Parrish, D. F. and Derber, J. C.: The National Meteorological Center's spectral statistical-interpolation analysis system, Mon. Weather Rev., 120, 1747–1763, 1992.

Pielke, R. A. and Uliasz, M.: Use of meteorological models as input to regional and mesoscale air quality models – limitations and strengths, Atmos. Environ., 32, 1455–1466, 1998.

Skamarock, W. C.: Evaluating Mesoscale NWP models using kinetic energy spectra, Mon. Weather Rev., 132, 3019–3032, 2004.

Skamarock, W. C., Klemp, J. B., Dudhia, J., Gill, D. O., Barker, D. M., Wang, W., and Powers, J. G.: A description of the advanced research WRF version 2, NCAR Technical Note, NCAR/TN-468+STR, 8 pp., 2005.

Seaman, N. L.: Meteorological modeling for air-quality assessments, Atmos. Environ., 34, 2231–2259, 2000.

Secretaria del Medio Ambiente del Distrito Federal (SMA-DF): Inventario de Emisiones 2006 de la Zona Metropolitana del Valle de México, México, 2008.

Song, J., Lei, W., Bei, N., Zavala, M., de Foy, B., Volkamer, R., Cardenas, B., Zheng, J., Zhang, R., and Molina, L. T.: Ozone response to emission changes: a modeling study during the MCMA-2006/MILAGRO campaign, Atmos. Chem. Phys. Discuss., 9, 23419–23463, 2009, http://www.atmos-chem-phys-discuss.net/9/23419/2009/.

Stensrud, D. J., Bao, J.-W., and Warner, T. T.: Ensemble forecasting of mesoscale convective systems, paper presented at 12th Conference on Numerical Weather Prediction, Am. Meteorol. Soc., Phoenix, AZ, 11–16 January 1998.

Streit, G. E. and Guzman, F.: Mexico City air quality: progress of an international collaborative project to define air quality management options, Atmos. Environ., 30, 723–733, 1996.

Thomas, S. J., Hacker, J. P., Desgagne, M., and Stull, R.: An enemble analysis of forecast errors related to floating point performance, Weather Forecast., 17, 898–906, 2002.

Tie, X., Madronich, S., Li, G., Ying, Z., Zhang, R., Garcia, A., Lee-Taylor, J., and Liu, Y.: Characterization of chemical oxidants in Mexico City: A regional chemical dynamical model (WRFChem) study, Atmos. Environ., 41, 1989–2008, 2007.

Tribbia, J. J. and Baumhefner, D. P.: Scale interactions and atmospheric predictability: an updated perspective, Mon. Weather Rev., 132, 703–713, 2004.

Toth, Z. and Kalnay, E.: Ensemble forecasting at NMC: the generation of perturbations, B. Am. Meteorol. Soc., 74, 2317–2330, 1993.

Toth, Z. and Kalnay, E.: Ensemble forecasting at NCEP: the breeding method, Mon. Weather Rev., 125, 3297–3318, 1997.

Vukicevic, T. and Errico, R. M.: The influence of artificial and physical factors upon predictability estimates using a complex limited-area model, Mon. Weather Rev. 118, 1460–1482, 1990.

Wandishin, M. S., Mullen, S. L., Stensrud, D. J., and Brooks, H. E.: Evaluation of a short-range multi-model ensemble system, Mon. Weather Rev., 129, 729–747, 2001.

Wellens, A., Moussiopoulos, N., Sahm, P.: Comparisons of a diagnostic model and MEMO progrognostic model to calculate wind fields in Mexico City, in: Second International Conference on Air Pollution, Computational Mechanics Publ., Barcelona, Spain, 27–28, 1994.

Williams, M. D., Brown, M. J., Cruz, X., Sosa, G., and Streit, G.: Development and testing of meteorology and air dispersion models for Mexico City, Atmos. Environ., 29, 2929–2960, 1995.

Zhang, F., Bei, N., Nielsen-Gammon, J. W., Li, G., Zhang, R., Stuart, A. L., and Aksoy, A.: Impacts of meteorological uncertainties on ozone pollution predictability estimated through meteorological and photochemical ensemble forecasts, J. Geophys. Res., 112, D04304, doi:10.1029/2006JD007429, 2007.

Zhang, F., Snyder, C., and Rotunno, R.: Mesoscale predictability of the "surprise" 24–25 January 2000 snowstorm, Mon. Weather Rev., 130, 1617–1632, 2002.

Zhang, F., Snyder, C., and Rotunno, R.: Effects of moist convection on mesoscale predictability, J. Atmos. Sci., 60, 1173–1185, 2003.

Zhang, F., Odins, A. M., and Nielsen-Gammon, J. W.: Mesoscale predictability of an extreme warm-season precipitation event, Weather Forecast., 21, 149–166, 2006.

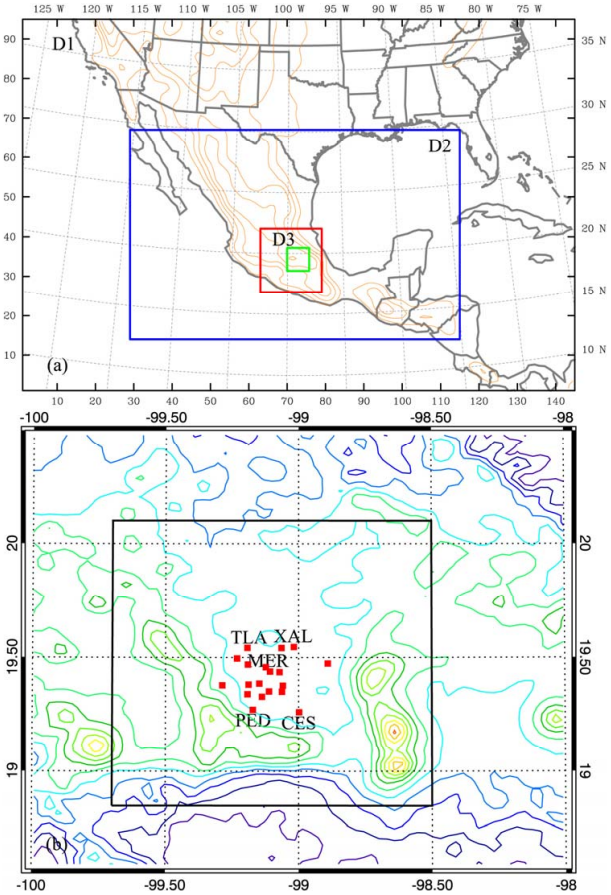

Fig. 1. (a) WRF domains (black, blue, red box) and **(b)** CAMx domain (green box in **a**, square signs are RAMA stations for ozone measurements). Inner box indicates the domain shown in Figs. 6 and 8. Contours in both panels represent terrain height.

ACPD
10, 3229–3263, 2010

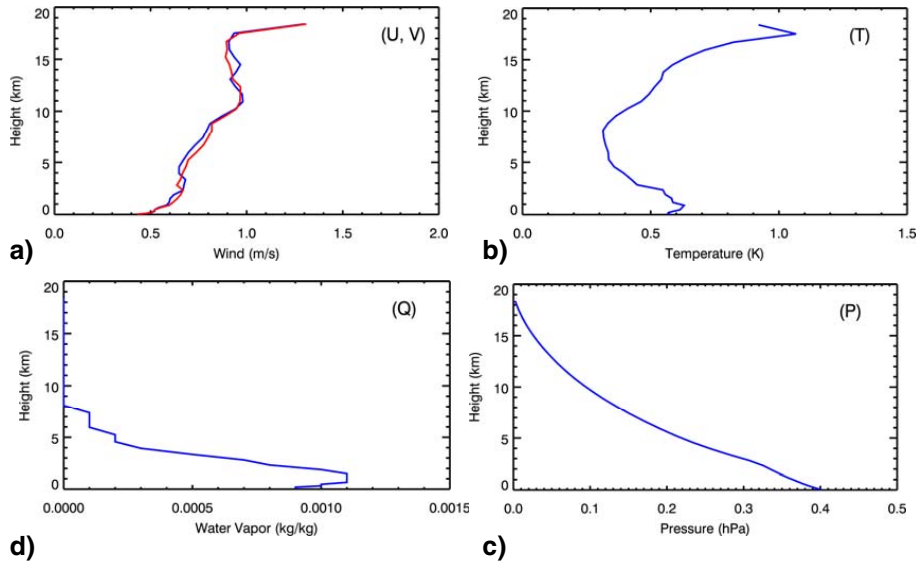

Fig. 2. Vertical distribution of the initial ensemble spread for **(a)** horizontal winds (u, v, m/s), **(b)** temperature (T, K), **(c)** pressure (p, hPa), and **(d)** water vapor mixing ratio (q, g/kg) over domain 1.

ACPD
10, 3229–3263, 2010

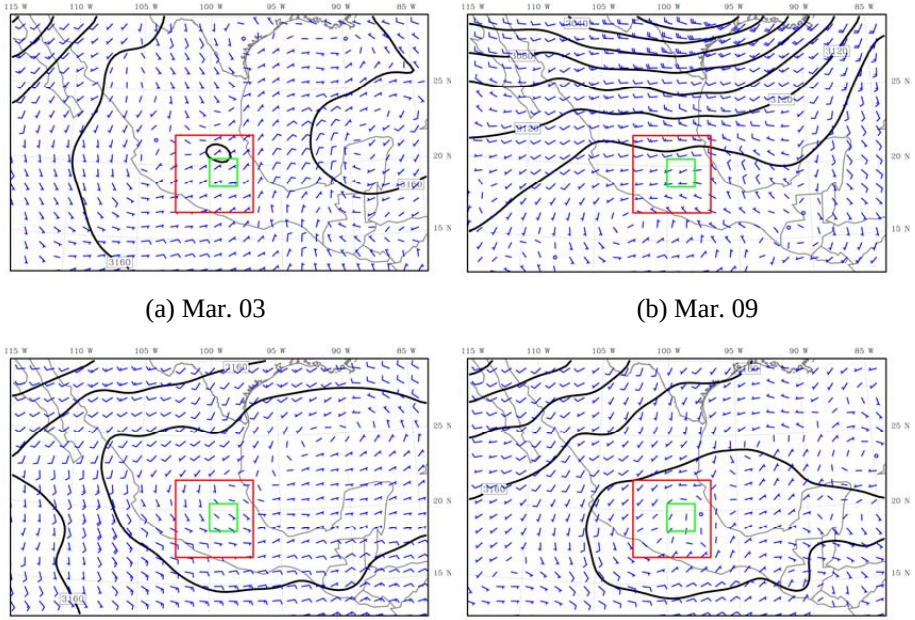

(a) Mar. 03 (b) Mar. 09

(c) Mar. 15 (d) Mar. 29

Fig. 3. The 700 hPa geopotential heights and winds at 12:00 CDT from GFS reanalysis data for **(a)** 3 March, **(b)** 9 March, **(c)** 15 March, and **(d)** 29 March 2006. Red box indicates domain3 used in WRF. Green box indicates the CAMx domain.

ACPD

10, 3229–3263, 2010

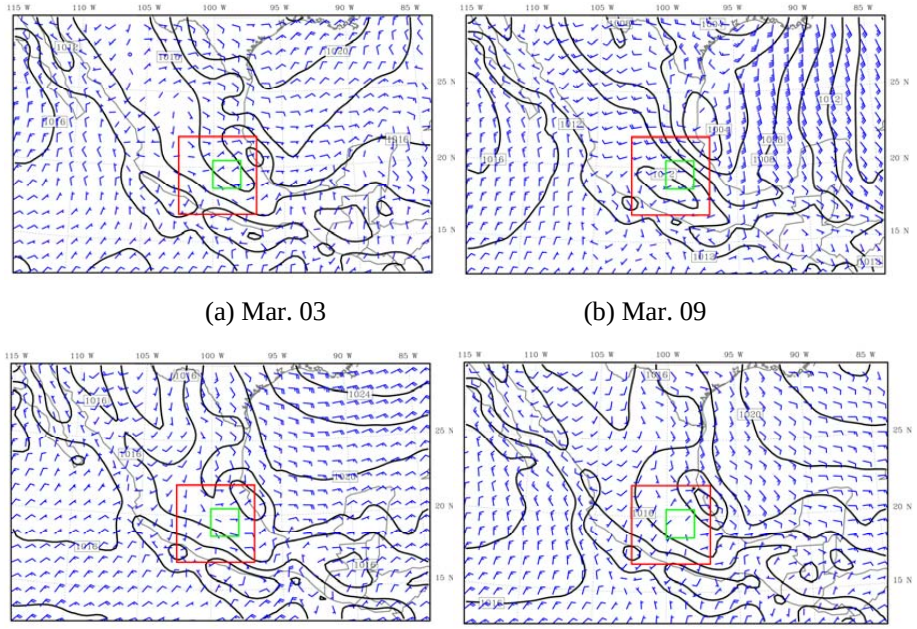

(a) Mar. 03 (b) Mar. 09

(c) Mar. 15 (d) Mar. 29

Fig. 4. As in Fig. 3, but for surface pressure and winds.

ACPD

10, 3229–3263, 2010

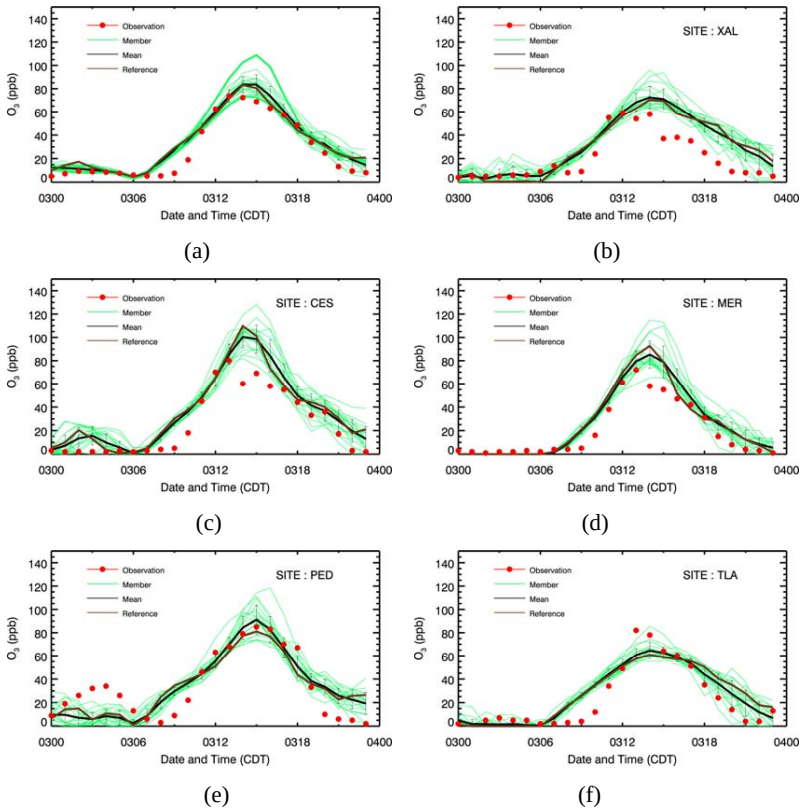

Fig. 5. Time evolution of the surface [O_3] (ppb) from each ensemble member (thin green lines) in (a), ensemble mean (bold black line) and reference deterministic forecast (bold orange line) of the CTRL ensemble simulation (3 March 2006) and observations (red dots) for **(a)** values averaged over the RAMA sites and **(b)** the 5 selected stations (TLA, XAL, MER, PED, and CES, shown in Fig. 1b). The error bars denotes the ensemble spread. Bold green lines in (a) indicate two extreme cases (low ozone case: EN-11 and high ozone case: EN-14).

ACPD
10, 3229–3263, 2010

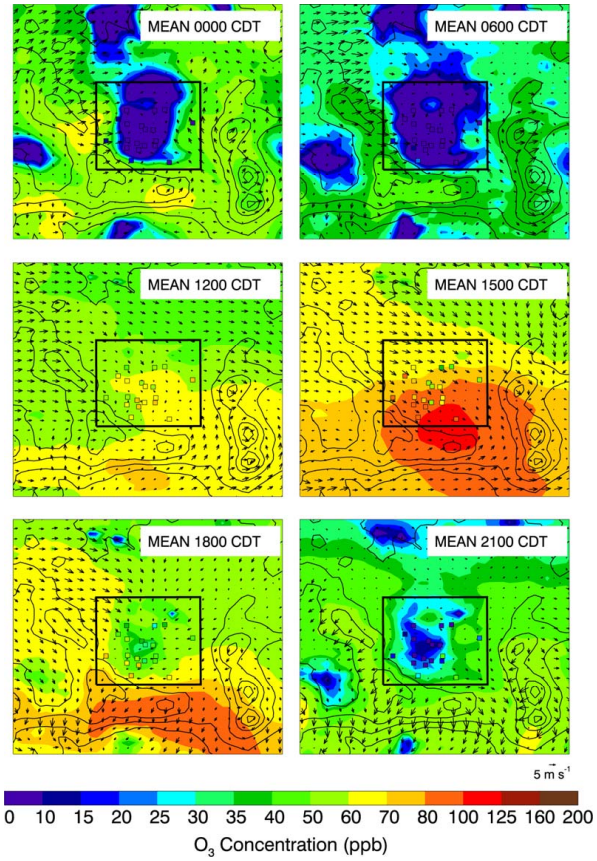

Fig. 6. Ensemble mean (color) of the surface [O_3] (ppb) distributions along with the ensemble mean winds valid at 00:00 CDT, 06:00 CDT, 12:00 CDT, 15:00 CDT, 18:00 CDT, and 21:00 CDT of the CNTL ensemble simulations (3 March 2006). The colored squares denote the ozone measurements from the RAMA sites.Inner box denotes the domain used for Fig. 7.

ACPD
10, 3229–3263, 2010

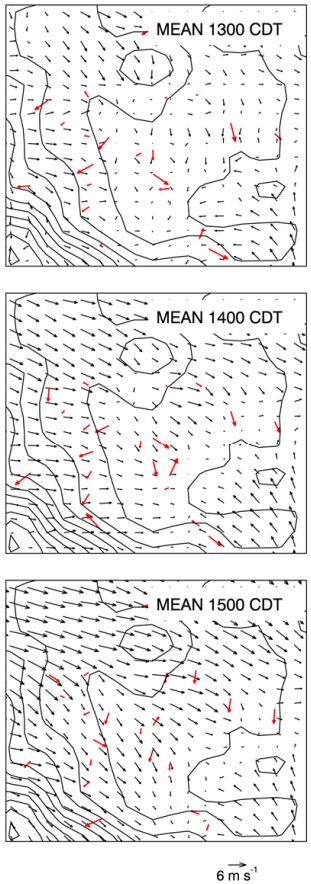

Fig. 7. Ensemble mean (black arrows) of the surface winds along with the measurements (red arrows) around the Mexico City basin for 13:00 CDT, 14:00 CDT, and 15:00 CDT on 3 March 2006.

ACPD
10, 3229–3263, 2010

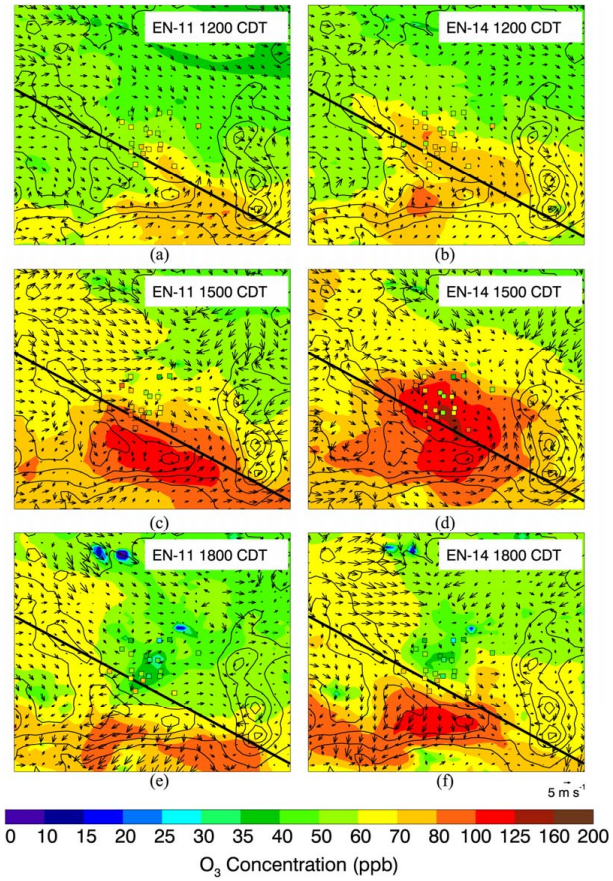

Fig. 8. Surface [O_3] (ppb) of two ensemble members (EN-11 and EN-14 shown in Fig. 5a) along with surface wind vectors valid at 12:00 CDT, 15:00 CDT, and 18:00 CDT on 3 March 2006. Cross line is the position of the cross-section shown in Fig. 9.

ACPD
10, 3229–3263, 2010

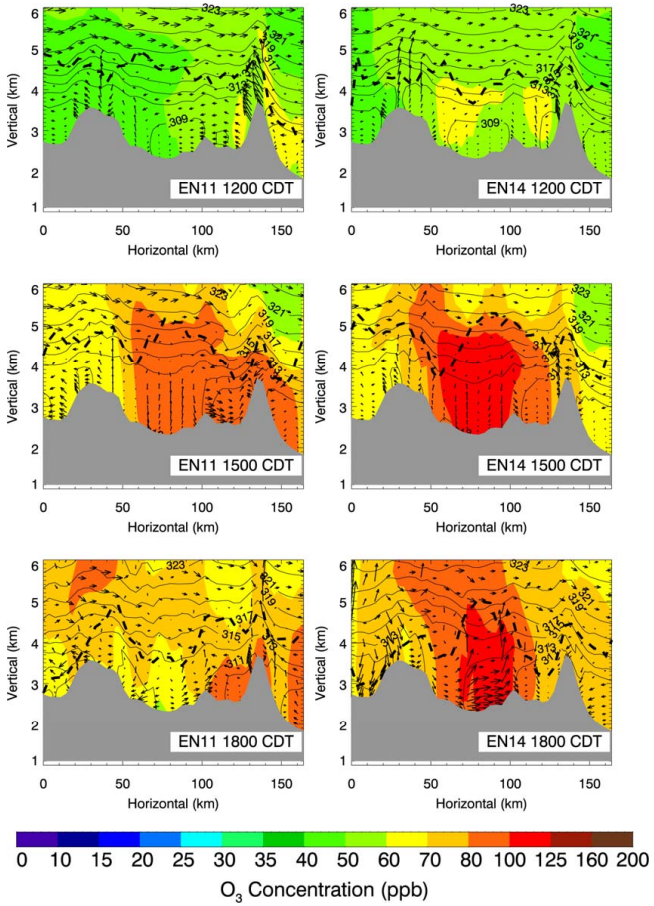

Fig. 9. Cross-section of [O_3] (ppb, shading), wind vectors, potential temperature (K, contours), and PBL height (km, bold dash line) of two ensemble members (EN-11 and EN-14) valid at 12:00 CDT, 15:00 CDT, and 18:00 CDT on 3 March 2006 along the cross line denoted in Fig. 8.

ACPD
10, 3229–3263, 2010

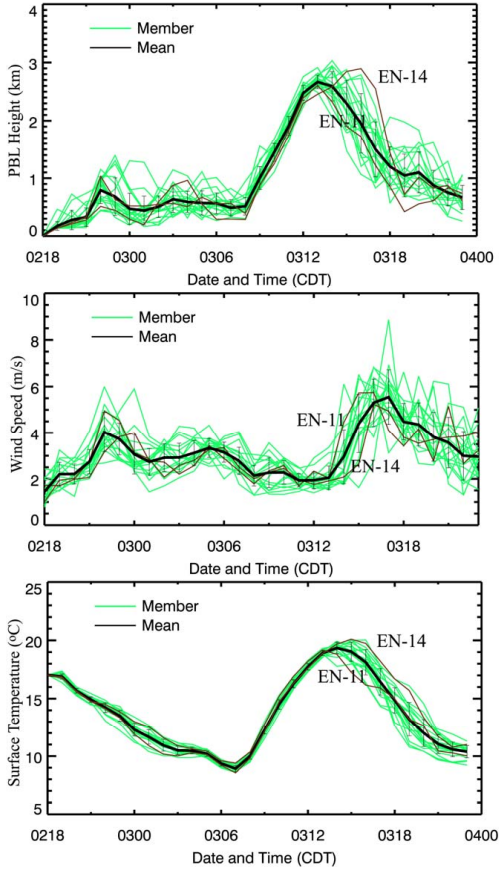

Fig. 10. Time evolution of the PBL height (km, top panel), wind speed (m/s, middle panel), and surface temperature (°C, bottom panel) from each ensemble member (thin green lines) and ensemble mean (bold black line) of the CTRL ensemble simulation (3 March 2006), two thin orange lines indicate two extreme members (EN-11 and EN-14).

ACPD
10, 3229–3263, 2010

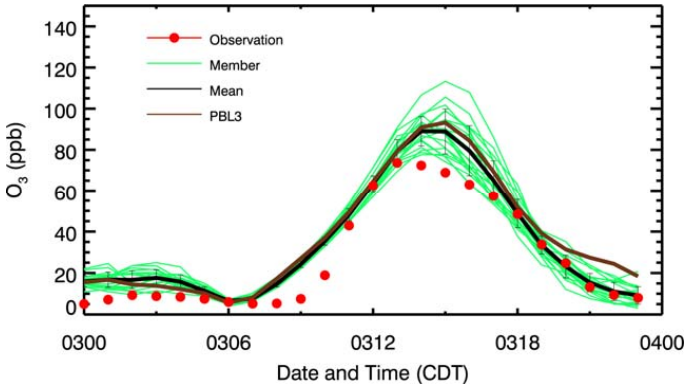

(a)

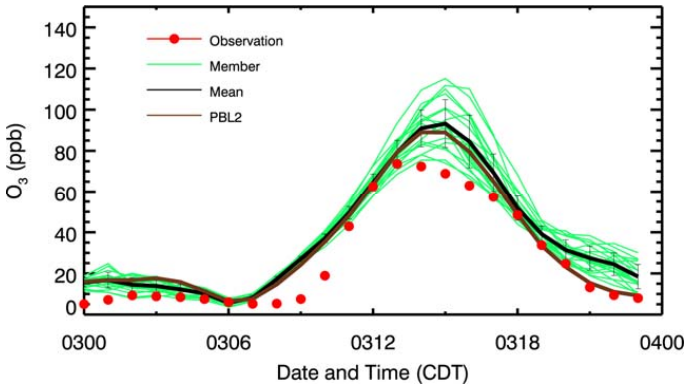

(b)

Fig. 11. Time evolution of the surface [O_3] (ppb) from each ensemble member (thin green lines), ensemble mean (bold black line) and reference deterministic forecast (bold orange line) of 3 March 2006 with other **(a)** PBL2: YSU scheme, **(b)** PBL3: MRF scheme, and observations (red dots) averaged over the RAMA sites. The error bars denotes the ensemble spread.

ACPD
10, 3229–3263, 2010

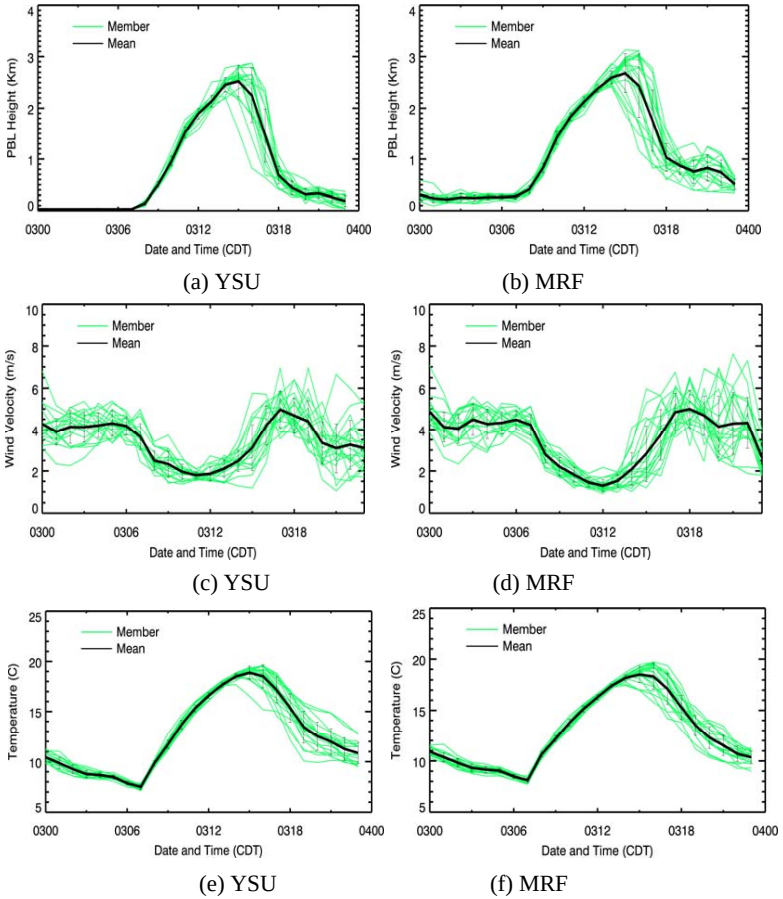

Fig. 12. Time evolution of the PBL height, wind speed, and surface temperature from each ensemble member (thin green lines) and ensemble mean (bold black line) of 3 March 2006 with YSU scheme **(a, c, e)** and MRF scheme **(b, d, f)**.

ACPD
10, 3229–3263, 2010

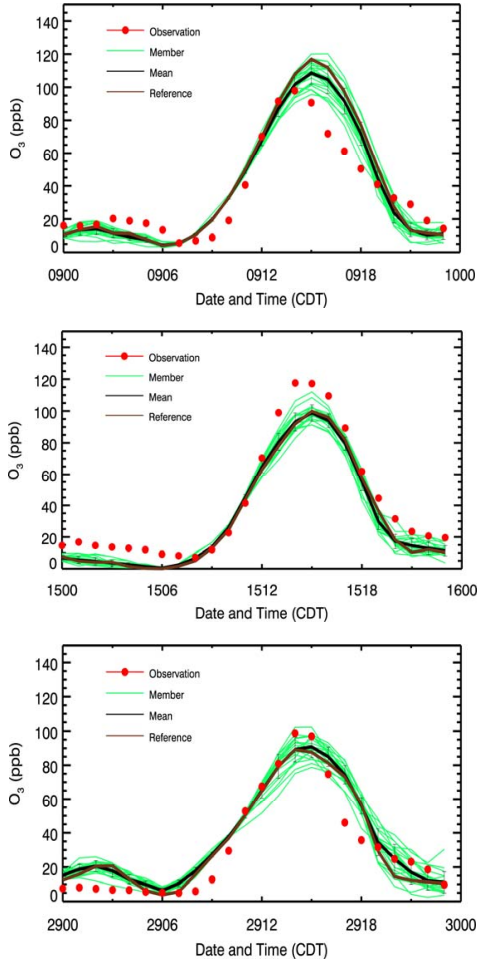

Fig. 13. As in Fig. 11 but for 9 March, 15 March, and 29 March 2006.

ACPD
10, 3229–3263, 2010